# Extended Skyrmion Phase in Epitaxial FeGe(111) Thin Films

S. X. Huang and C. L. Chien

Phys. Rev. Lett. **108**, 267201 — Published 26 June 2012

DOI: 10.1103/PhysRevLett.108.267201

# Extended Skyrmion Phase in Epitaxial FeGe(111) Thin Films

S. X. Huang* and C. L. Chien*

*Department of Physics and Astronomy, The Johns Hopkins University, Baltimore, Maryland 21218, USA*

Abstract

The skyrmion state in epitaxial B20 FeGe(111) thin films, determined by the topological Hall effect, is greatly extended in the phase diagram to cover all temperatures up to the Curie temperature $T_C \approx 271$ K and over a wide magnetic field range that includes zero magnetic field. The properties of the skyrmion phase can be controlled and manipulated by the film thickness, which has a strong effect on the stabilization of skyrmions.

Topological concepts have provided a fascinating twist to our understanding of ordering in physics. One intriguing example is the skyrmion spin texture [1, 2] which carries a topological charge and Berry phase in real space. These non-trivial spin textures are closely related to emergent electromagnetic phenomena [3] and exhibit spectacular dynamic properties [4-6]. Recently, non-centrosymmetric cubic B20 chiral magnets of metallic MnSi, $Fe_{1-x}Co_xSi$, FeGe and insulating $Cu_2OSeO_3$ (multiferroic) with broken space-inversion symmetry have received a great deal of attention. Exotic skyrmion spin textures have been observed in reciprocal space by small angle neutron scattering [2] and in real space by Lorentz transmission electron microscopy (TEM) [7-10]. In these 2D skyrmion double-twist textures, the spins twist smoothly along both the radial and angular directions. The spins rotate gradually from spin down at the center to spin up at the edge of a skyrmion along the radial direction, and rotate smoothly as a vortex along the angular direction. These nanoscale skyrmions tend to form a lattice with hexagonal symmetry The Berry phase acquired by the electrons traversing through a skrymion may be exploited in new spintronics devices due to its unusual response to electric charge current and spin current (e.g. five orders lower current density to move a skyrmion than that required for spin transfer torque switch of regular ferromagnets) [11-13]. In bulk B20 ferromagnets, non-collinear helical spin structures with wavelength $\lambda_H$ are favored by the Dzyaloshinskii-Moriya (DM) interaction. Under the DM interaction with a chiral energy of $D\mathbf{M}\bullet(\nabla\times\mathbf{M})$, where $D$ is the Dzyaloshinskii constant, skyrmion-like spin structures (precursor states) are formed by thermal fluctuations but only in a very small region in the phase space at temperatures $T$ close to, but below, the ferromagnetic transition temperature $T_C$ and with the presence of a magnetic field $H$ [1, 2, 14]. Such a small region in phase space is unattractive, and indeed impedes the exploration of skyrmion physics. However, the regular skyrmion phase may be greatly expanded in thin

specimens, especially in thin films [7]. In Lorentz TEM studies of $Fe_{0.5}Co_{0.5}Si$ [7], FeGe[8], MnSi[9], and $Cu_2OSeO_3$ [10] using specimens with thickness $t$ < 100nm that have been ion-milled from bulk crystals, skyrmions have been found to stabilize in a much wider ($T$, $H$) region than those in bulk crystals. Theoretical studies in chiral magnets indicate that uniaxial distortion can greatly stabilize skyrmions over a much wider region in phase space extending to near zero temperature, and possibly even at zero magnetic field [15-20].

These encouraging experimental and theoretical suggestions notwithstanding, studies of the rich physics of skyrmions have thus far been confined mostly to bulk materials. It is imperative to explore thin films of chiral magnets and explore the modification of the skyrmion phase. Large epitaxial thin films of specific orientations are particularly beneficial in the absence of large single crystals. For the exploration of new spintronic phenomena in skyrmions, thin films are also much more useful where patterned structures are essential.

Among the known cubic B20 chiral magnets, FeGe has the highest $T_C \approx 278$K with $\lambda_H$ of about 70 nm along the helical propagation vector, whose direction is temperature dependent [21]. Under a magnetic field of about 300 Oe, the helical spin structure changes into the conical phase with the propagation vector along the field direction [21]. At the saturation field $H_D \approx D^2\mathbf{M}/2A \approx$ 3 kOe at low temperatures, where $A$ is the exchange stiffness, the conical phase transforms into ferromagnetic alignment [21]. Similar to MnSi and $Fe_{0.5}Co_{0.5}Si$, bulk B20 FeGe also has a very small (T,H) region for the skyrmion-like (precursor states) phase [22]. Unlike MnSi and $Fe_{0.5}Co_{0.5}Si$, for which large single crystals exist, only mm-size FeGe single crystals are available. The lack of large single crystals impedes studies of FeGe despite favorable attributes. We report in this work the realization of epitaxial FeGe thin films, with which we show that the

skyrmion structures can be stabilized in a dramatically larger ($T$,$H$) region including zero magnetic field, even in films with $t > \lambda_H$.

Epitaxial FeGe(111) films, 18-300 nm in thickness, have been grown by magnetron sputtering in a high vacuum chamber (base pressure $3.5 \times 10^{-8}$ torr) on HF etched undoped Si(111) substrates at a substrate temperature of 500 ºC. The $\theta/2\theta$ x-ray diffraction pattern (not shown) indicates only the B20 FeGe(111) phase with less than 0.5% impurity phases. The out-of-plane lattice constant $d_{111}$ is about 0.5% less than that in bulk and indicats tensile strain. X-ray diffraction $\phi$-scan reveals the epitaxial relationship of FeGe[1$\underline{1}$0] || Si[11$\underline{2}$] with a 30º rotation and twinning as shown in Fig. 1a over the area of 3 $cm^2$.

Magnetic hysteresis loops at 10 K of the 300-nm FeGe film with in-plane ($H_{||}$) and out-of-plane ($H_{\perp}$) magnetic fields reveal in-plane magnetization favored by shape anisotropy as shown in Fig. 1b. The saturation field $H_S$, defined at the knee point in the $M$-$H$ curve, is about 1.5 kOe and 7 kOe for $H_{||}$ and $H_{\perp}$ respectively. The in-plane saturation field of 1.5 kOe is considerably smaller than the $H_D \approx 3$ kOe defined above, suggesting more complex ordering such as the helicoid phase [19] under $H_{||}$. In contrast to those of common ferromagnets such as Fe and Co, the $H_{||}$ hysteresis loop of FeGe film shows negligible remenance, a small coercivity and a slanted loop, features that are likely to be related to the complex domain structures of the helicoids [23-25]. The ac susceptibility measurement with an in-plane ac field of 10 Oe at 913Hz (inset of Fig. 1b) gives $T_C \approx 271$ K, slightly lower than that of bulk FeGe. The resistance measurements show that all the FeGe films are metallic displaying a systematic dependence on thickness. The high resistance ratio $R$(300 K)/$R$(10 K) of 7 for the 300-nm film, suggests high quality FeGe(111) epitaxial films. As shown in the inset Fig. 1c, the resistivity at room

temperature of the FeGe thin films varies little for the thick films but increases sharply at small thicknesses as interfacial scattering sets in.

The skyrmion spin texture in B20 chiral magnets has skyrmion number -1 [2], where each skyrmion quantizes with an emergent gauge flux of 2 flux quanta ($2\Phi_0=h/e$) [8]. This quantization produces a fictitious magnetic field of $B_{eff}=2\Phi_0/A$, where $A$ is the area of the skyrmion, that deflects electrons and leads to the topological Hall effect (THE) [26, 27]. Numerous experiments [12, 28-30] have demonstrated that THE is strong evidence, indeed a hallmark, for the existence of skyrmions. The total Hall resistivity $\rho_H$ is then [30]:

$$\rho_{yx} = \rho_H = R_0 H + R_S M + \rho_{TH} \qquad (1)$$

where $R_0$ is the ordinary Hall coefficient, $R_S$ is the anomalous Hall effect (AHE) coefficient, $\rho_{TH}$ is the topological Hall resistivity due to the skyrmion spin texture, and $H$ is perpendicular to the film plane. In Eq.(1), the magnetization value $M$ includes only that of the sample with the substrate contribution separately measured and subtracted. It turns out that the analysis of extracting $\rho_{TH}$ is insensitive to any residue linear M-H contribution, which affects the value of $R_0$ but not those of $\rho_{TH}$. While $R_S$ may be a complex function of resistivity $\rho$ (e.g., $a\rho+b\rho^2$) [31], in our case, the magnetoresistance (MR) is so small (less than 0.5%) that the detailed mechanisms for AHE are irrelevant ($R_S$ is nearly a constant with magnetic field). For simplicity, we adopt $R_S=S_A\rho^2$ as in previous works, where $S_A$ is independent of magnetic field [30, 32]. At large $H$, $\rho_{TH}$ vanishes when all the spins are aligned. Following previous analyses [30], by a linear fitting of $\rho_H/H$ vs $\rho^2 M/H$ at large fields, we obtained the coefficients $R_0$ and $S_A$. The resistivity $\rho_{TH}$ due to THE can then be obtained by subtracting ($R_0H+R_SM$) from $\rho_H$. The value $S_A$ obtained for the FeGe thin films is positive, whereas it is negative for MnSi [32] and positive for $Fe_{1-x}Co_xSi$ [33].

As shown in Fig. 2a (field sweeps from positive to zero), at high fields of $H > H_{skx} \approx 14$ kOe, the calculated and experimental $\rho_H$ results agree excellently.

The experimental $\rho_H$ data (in black) for the 60-nm FeGe film measured at 10 K are shown in Fig. 2a. The calculated $R_0H+R_SM$ values (in red) using the best-fit values of $R_0$ and $R_S$ also increases monotonically with $H$ and coincides with $\rho_H$ (in black) at high fields after THE has been eliminated. By subtracting ($R_0H+R_SM$) (in red) from the experimental $\rho_H$ data (black curve), we obtain the THE contribution $\rho_{TH}$ (in blue), which shows a dome with a minimum at $H_m$. Such a dome shape of $\rho_{TH}$ centered at $H_m$ is unique to THE and has been observed in previous experiments [28-30] and described in theories [34]. Lorentz TEM measurements [7, 8] with an out-of-plane field reveal the evolution of the magnetic phases culminating with the formation of the skyrmion lattice at $H_m$. Below $H_m$, stripe domain (helicoid) and skyrmions coexist, whereas $H$ higher than $H_m$ suppresses the skyrmion phase and eventually leads to the fully magnetized state. Interestingly, the value of $H_{skx}$ is much larger than that of $H_S$. This is likely due to the formation of free isolated (repulsive) skyrmions, which are excitations of the saturated state and exist as topologically stable 2D solitons at fields far above $H_S$ as predicted in theory [19].

To describe the relative magnitude of THE, we use $\mathrm{THR_m} = \rho_{TH}(H_m)/\rho_H(25\ kOe)$, the ratio of $\rho_{TH}(H_m)$ at the peak of the dome and the Hall resistivity $\rho_H(25\ kOe)$ at large field when THE is absent. We have found $\mathrm{THR_m} \approx 25\%$ at 10 K and decreasing to 6% at 150 K, at which $R_oH$ is less than 1% of $\rho_H$. For all the FeGe films presented here, $\rho_{TH}$ shows a similar THE dome structure with $\mathrm{THR_m}$ larger than 20% at 10 K. At temperatures larger than $T_C$, e.g., 280 K, there is no THE as shown in Fig. 2b. The values of $R_0H+R_SM$ coincide with the experimental data (within 1%) at all magnetic fields.

We determine the skyrmion phase diagram according to the measured $\rho_{TH}$ for the epitaxial FeGe films. In bulk FeGe, there is a tiny skyrmion-like (precursor) region in the phase space within the temperature range of $\Delta T \approx 273 - 278$ K and the field range of $\Delta H \approx 0.1 - 0.5$ kOe as shown in the inset of Fig. 2c. In contrast, as shown in Fig. 2c and 2d, the skyrmion region ($T$,$H$) in FeGe thin films, illustrated by the 18-nm and 300-nm samples is dramatically expanded to cover essentially the entire temperature range from low temperatures to $T_C$. Furthermore, in bulk FeGe the skyrmion state emerges only under a magnetic field since the ground state is the conical (helical) state. In FeGe thin film the skyrmion state *exists* in the ground state even at zero magnetic field. At 10 K, the magnetic field range has extended to more than 10 kOe. Within the skyrmion phase, $\rho_{TH}$ varies systematically and reaches a maximum in the vicinity of 150 K, at which $\rho_{TH}$ = 0.16 and 0.08 μΩ·cm for the 18-nm and 300-nm films respectively. The THE resistivity, due to the fictitious magnetic field as a result of the skyrmion spin textures, is $\rho_{TH} = n_{skx} P R_o B_{eff}$ [27, 28], where $n_{skx}$ is the relative skyrmion density (for compact arrays, $n_{skx}$=1), and $P$ is the local spin polarization. For FeGe, $B_{eff}$ is about 1 T if we take the skyrmion size as 70 nm. The value of $R_o$ = 0.072 μΩ·cm/T, measured well above $T_C$ at $T$=380 K for the 300-nm film, gives a value of $R_o B_{eff}$ = 0.072 μΩ·cm, in good agreement with the experimental value of 0.08 μΩ·cm. For a thinner film (18-nm), the skyrmion size may be smaller [35], thus resulting in larger $B_{eff}$ and $\rho_{TH}$. Assuming that $P$, $R_o$, and $B_{eff}$ are independent of temperature, the variation of $\rho_{TH}$ reflects that of $n_{skx}$. This variation of $n_{skx}$ is in good agreement with the Lorentz TEM measurement of a wedged FeGe thin specimen (15 nm to 75 nm wedge in thickness by ion-milling of polycrystalline FeGe) [8], where $n_{skx}$ reaches a maximum at around 150 K - 200 K in the intermediate fields and is smaller at low temperature for the 15 nm region. However, for the 75 nm ($\sim\lambda_H$) region, skyrmions exist only in a very small ($T$,$H$) region close to

$T_C$ [8]. In our epitaxial thin films, even for the 300 nm film (~ 4 $\lambda_H$), skyrmions exist in a much extended (*T*,*H*) region, essentially over the entire temperature range below $T_C$. In recent Lorentz TEM studies of MnSi and $Cu_2OSeO_3$ at which the thicknesses of thin specimens are 2-3 times their wavelengths, the skyrmion phases also exist in a much extended (*T*,*H*) region[9, 10].

In Fig. 2c and 2d, the red lines indicate the values of $H_m$ at various temperatures. It is noted that the $H_m$ value for the 300-nm film is about twice the value for the 18-nm film, i.e., the thicker film has a larger skyrmion region, in contrast to that in ref.[8]. To understand the underlying mechanism for stabilizing skyrmions in thin films, we have carried out measurements of thin films of various thicknesses from 18 nm to 300 nm. The field dependence of the THR (= $\rho_{TH}/\rho_H(25\ kOe)$) shows a systematic variation with thickness as shown in Fig. 3a, where $H_m$, at the bottom of the dome, progressively shifts to higher *H* for increasing *t* thus confirming larger skyrmion region in thicker films.

Theories suggest that the uniaxial anisotropy in B20 chiral magnets plays an essential role [15-19] in the stabilization of skyrmions. The uniaxial anisotropy *K* (*K* >0 favoring perpendicular magnetic anisotropy (PMA) with an energy of $-KM_z^2$) and "effective stiffness" $K_0$ of the conical phase can be calculated from the in-plane and out-of-plane saturation field $H_{||S}$ and $H_{\perp S}$ [20]:

$$K = -\frac{M_S}{3}\left(H_{\perp S} - H_{||S} - 4\pi M_S - \frac{K_m}{M_S}\right),$$

$$K_0 = \frac{M_S}{6}\left(H_{\perp S} + 2H_{||S} - 4\pi M_S + \frac{2K_m}{M_S}\right),$$

$$K_m = M_s^2 \frac{\lambda_H}{t}(1 - \exp(-2\pi t/\lambda_H)). \qquad (2)$$

In the case of 300-nm film, we obtain $K/K_0 \approx 0.02$. As shown in the inset of Fig. 3a, $K$ increases for decreasing thickness $t$ and reaches to 1.1 for $t$=18 nm. The increasing PMA, as in other magnetic thin films, may originate from surface effects and/or magneto-elastic anisotropy [36] and requires further studies.

The stabilization of skyrmions in our epitaxial films, and the dependence of $H_m$ on $t$, are likely due to the positive $K$ as suggested in theoretical calculations [18]. The conical phase is suppressed due to the increasing DM energy under a positive $K$, whose magnitude can be as low as $0.05K_0$. As a result, skyrmions have the lowest energy under a positive $K$ and a magnetic field. A larger $K$ (up to ~2.5 $K_0$) requires a smaller magnetic field ($H_m$) to "trigger" the skyrmion lattice and results a smaller $H$-$T$ region of skyrmion phase [18]. Our experimental results are consistent the theoretical phase diagram in ref. [18]. As shown in Fig. 3b, the largest $\rho_{TH}$ occurs at the smallest $t$, perhaps due to the smaller skyrmion size in thinner films [35].

As shown in Fig. 2 and Fig. 3, when the magnetic field is swept from positive to zero the topological Hall resistivity reduces to a small but negative value at zero magnetic field. The nonzero $\rho_{TH}$ at zero field observed in our epitaxial films, which is not observed in bulk samples[28-30], may come from the pinning of skyrmions by grain boundaries, such as the 'half-skyrmion'-like structure pinned at the grain boundary at zero field observed in Lorentz TEM experiments [8]. This result suggests not only the existence of skyrmions at zero field, but also the unusual behavior at $H = 0$ between the H-increasing and the H-decreasing branches. In Fig. 1a, the magnetization of FeGe film shows a normal counterclockwise hysteresis loop with a small positive remnant magnetization $M_r$ when $H$ is swept from large positive $H$ to zero, which is denoted as $H = 0^+$. From Eq.(1), the Hall resistivity at $H = 0^+$ is $\rho_H(0^+) = R_S M_r + \rho_{TH}(0^+)$, which

is negative because $M_r$ is small and $\rho_{TH}(0^+) < 0$ as shown in Fig. 3a. By the same token, when $H$ is swept from large negative $H$ to zero, denoted as $H = 0^-$, $\rho_H(0^-) = -\rho_H(0^+) > 0$. As a result, the Hall resistivity shows a hysteresis loop that is clockwise as shown Fig. 4.

In summary, despite existing in a very small region of the phase space in bulk FeGe, the skyrmion phase has been greatly expanded in epitaxial FeGe(111) thin films, in agreement with theoretical studies[15-19]. In FeGe thin films, the skyrmion phase exists over the entire temperature range up to $T_C$ and over a wide magnetic field range that includes zero field. The skyrmion phase is present in films from 18 nm to at least 300 nm, which is several times the wavelength. Epitaxial skyrmion thin films open the way for studies of skyrmions, the manipulation of their properties and the exploration of new spintronic properties of skyrmion.

Acknowledgements: We thank Professor Oleg Tchernyshyov for helpful discussions. This work is supported by the NSF under DMR-0520491 and DMR-0821005.

*To whom correspondence should be addressed:

sxhuang@pha.jhu.edu

clc@pha.jhu.edu

Reference:

[1] U. K. Roszler, A. N. Bogdanov, and C. Pfleiderer, Nature **442**, 797 (2006).
[2] S. Mühlbauer *et al.*, Science **323**, 915 (2009).
[3] N. Nagaosa, and Y. Tokura, Phys Scripta **2012**, 014020 (2012).
[4] O. Petrova, and O. Tchernyshyov, Physical Review B **84**, 214433 (2011).
[5] M. Mochizuki, Physical Review Letters **108**, 017601 (2012).
[6] Y. O. Y. Onose, S. Seki, S. Ishiwata, Y. Tokura, ArXiv **1204.5009**, (2012).
[7] X. Z. Yu *et al.*, Nature **465**, 901 (2010).
[8] X. Z. Yu *et al.*, Nat Mater **10**, 106 (2011).
[9] A. Tonomura *et al.*, Nano Letters **12**, 1673 (2012).
[10] S. Seki *et al.*, Science **336**, 198 (2012).
[11] F. Jonietz *et al.*, Science **330**, 1648 (2010).
[12] T. Schulz *et al.*, Nat Phys **8**, 301 (2012).
[13] J. Zang *et al.*, Physical Review Letters **107**, 136804 (2011).
[14] C. Pappas *et al.*, Physical Review Letters **102**, 197202 (2009).
[15] A. Bogdanov, and D. Yablonsky, Sov. Phys. JETP **68**, 101 (1989).
[16] A. Bogdanov, and A. Hubert, J Magn Magn Mater **138**, 255 (1994).
[17] A. Bogdanov, and A. Hubert, J Magn Magn Mater **195**, 182 (1999).
[18] A. B. Butenko *et al.*, Physical Review B **82**, 052403 (2010).
[19] U. K. Rößler, A. A. Leonov, and A. N. Bogdanov, Journal of Physics: Conference Series **303**, 012105 (2011).
[20] E. A. Karhu *et al.*, Physical Review B **85**, 094429 (2012).
[21] B. Lebech, and et al., Journal of Physics: Condensed Matter **1**, 6105 (1989).
[22] H. Wilhelm *et al.*, Physical Review Letters **107**, 127203 (2011).
[23] M. Uchida *et al.*, Science **311**, 359 (2006).
[24] M. Uchida *et al.*, Physical Review B **77**, 184402 (2008).
[25] F. Li, T. Nattermann, and V. L. Pokrovsky, Physical Review Letters **108**, 107203 (2012).
[26] J. Ye *et al.*, Physical Review Letters **83**, 3737 (1999).
[27] P. Bruno, V. K. Dugaev, and M. Taillefumier, Physical Review Letters **93**, 096806 (2004).
[28] A. Neubauer *et al.*, Physical Review Letters **102**, 186602 (2009).
[29] M. Lee *et al.*, Physical Review Letters **102**, 186601 (2009).
[30] N. Kanazawa *et al.*, Physical Review Letters **106**, 156603 (2011).
[31] N. Nagaosa *et al.*, Reviews of Modern Physics **82**, 1539 (2010).
[32] M. Lee *et al.*, Physical Review B **75**, 172403 (2007).
[33] Y. Onose *et al.*, Physical Review B **72**, 224431 (2005).
[34] S. D. Yi *et al.*, Physical Review B **80**, 054416 (2009).
[35] N. S. Kiselev *et al.*, Journal of Physics D: Applied Physics **44**, 392001 (2011).
[36] M. T. Johnson *et al.*, Reports on Progress in Physics **59**, 1409 (1996).

Figure captions:

Fig.1 (Color online). (a) In-plane φ scan about the (111) peak of FeGe(111) film and Si(111) substrate, (b) Hysteresis loop of 300-nm FeGe film at 10 K. Inset: In-plane ac susceptibility of FeGe(111) film as a function of temperature. (c) Resistivity ratio $R$(T)/$R$(300K) as a function of temperature for films with various thicknesses indicated. Inset: resistivity at 300 K as a function of thickness.

Fig. 2 (Color online). Hall resistivity as a function of field for (a) 60-nm film at 10 K, and (b) 60-nm film at 150 K, inset: 240-nm at 280 K, showing experimental $\rho_H$ (black), calculated (red) values of $R_0H + R_SM$ according to eq.(1), and the topological Hall resistivity $\rho_{TH}$ (blue). Color map of topological Hall resistivity in $H$-$T$ plane for (c) 300-nm and (d) 18-nm film and the values of $H_m$. Inset of (c): skyrmion-like (precursor states) region for bulk FeGe from ref. [22]. Inset of (d): maximum values of ($-\rho_{TH}$) as a function of temperature.

Fig. 3 (Color online). (a) Normalized THR = $\rho_{TH}/\rho_H$*(25 kOe)* as a function of magnetic field for various thicknesses at 10 K. Insert: $K/K_0$ and $H_{\perp S}$ as a function of thickness $t$. (b) Color map of topological Hall resistivity in $H$-$t$ plane at $T$=10 K, square symbols are the values of $H_m$.

Fig. 4 (Color online). Hall resistivity hysteresis loop for 30-nm films at 10 K.

Fig.1

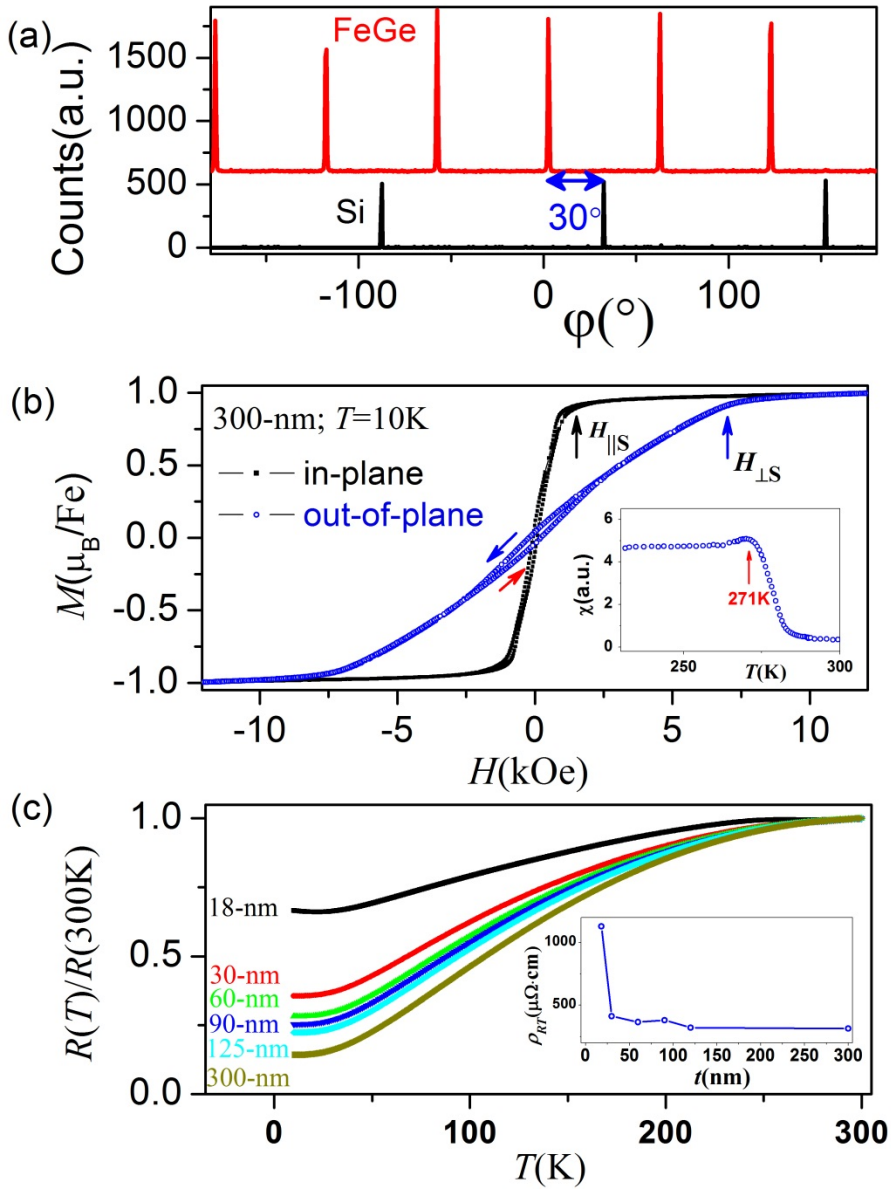
(a)
FeGe
Si
30°
Counts(a.u.)
1500
1000
500
0
-100
0
100
φ(°)
(b)
300-nm; T=10K
in-plane
out-of-plane
H||S
H⊥S
M(μB/Fe)
1.0
0.5
0.0
-0.5
-1.0
-10
-5
0
5
10
H(kOe)
χ(a.u.)
271K
T(K)
(c)
18-nm
30-nm
60-nm
90-nm
125-nm
300-nm
R(T)/R(300K)
T(K)
ρxx(μΩ.cm)
t(nm)

Fig.2

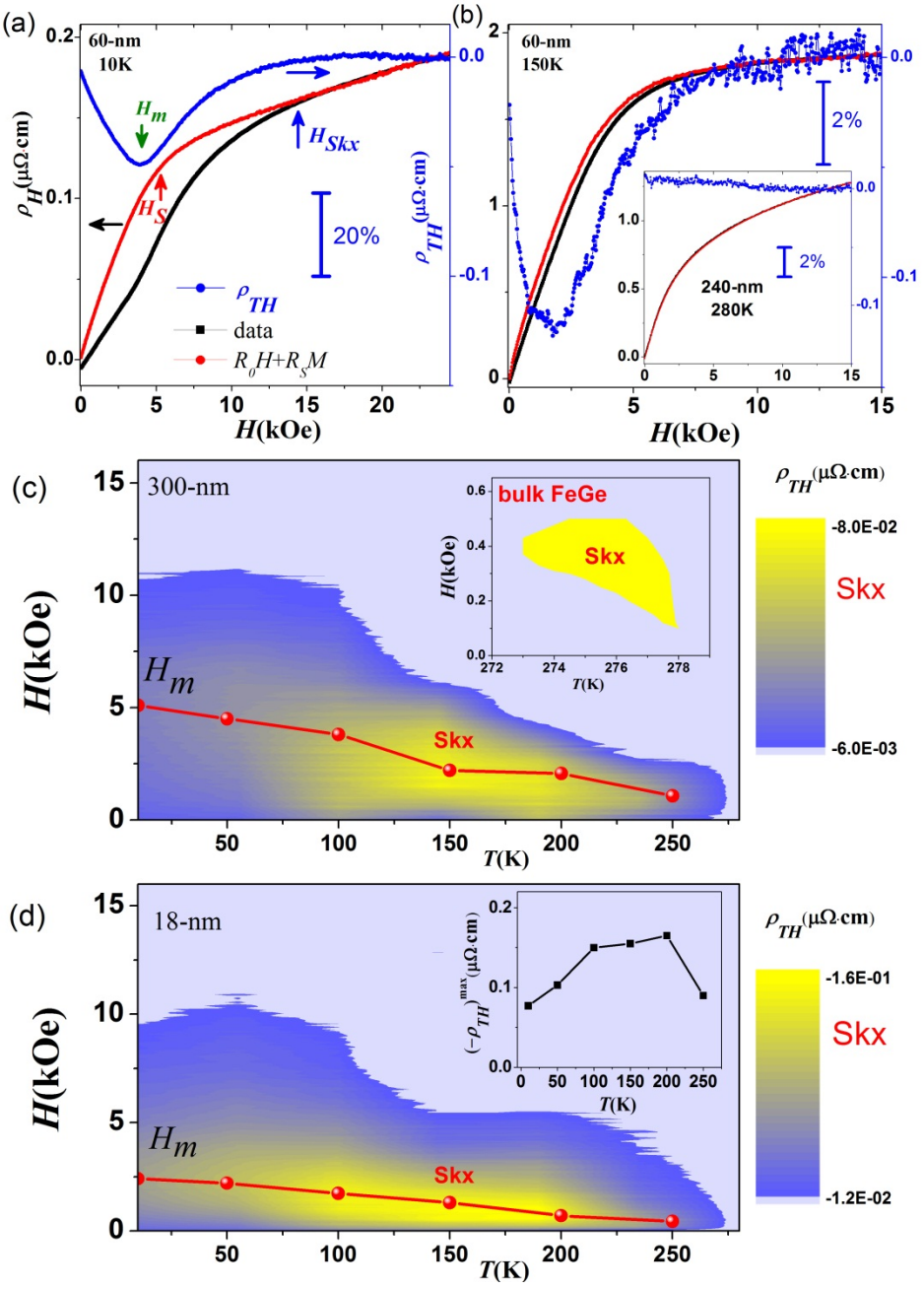
(a)
60-nm
10K
$H_m$
$H_{Skx}$
$H_S$
20%
$\rho_{TH}$
data
$R_0H+R_SM$
$\rho_H$(μΩ·cm)
$\rho_{TH}$(μΩ·cm)
H(kOe)
(b)
60-nm
150K
2%
240-nm
280K
2%
H(kOe)
(c)
300-nm
bulk FeGe
Skx
H(kOe)
T(K)
$H_m$
Skx
$\rho_{TH}$(μΩ·cm)
-8.0E-02
Skx
-6.0E-03
(d)
18-nm
$(-\rho_{TH})^{max}$(μΩ·cm)
T(K)
$H_m$
Skx
H(kOe)
$\rho_{TH}$(μΩ·cm)
-1.6E-01
Skx
-1.2E-02

Fig.3

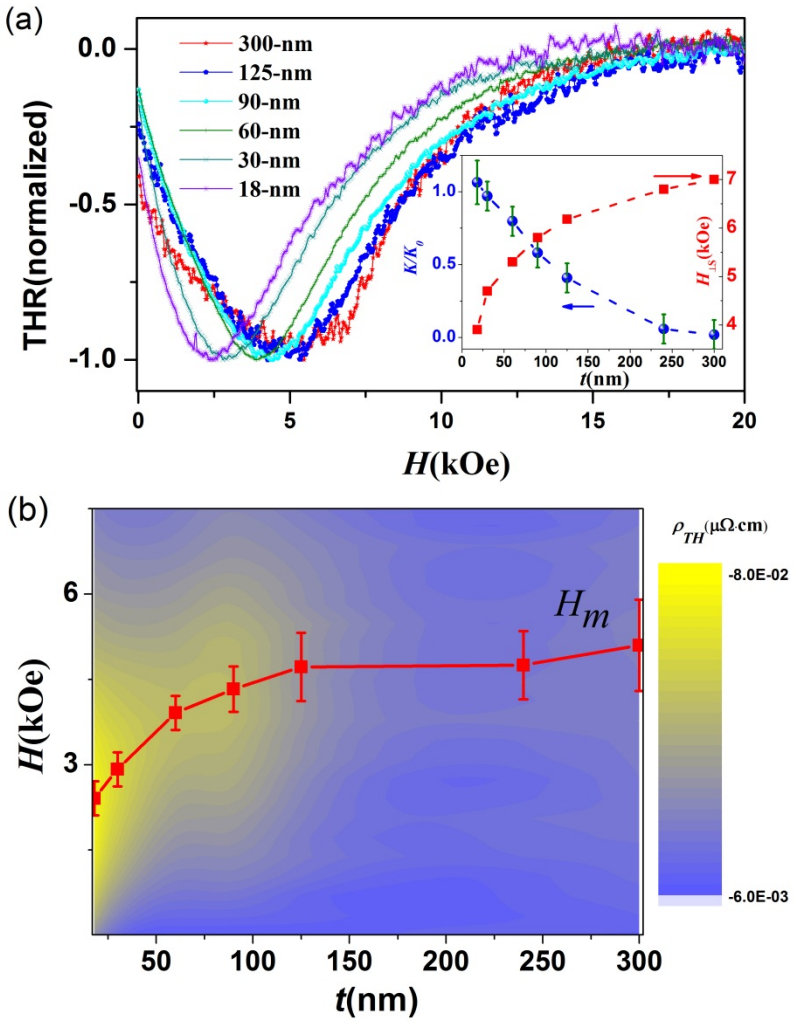
(a)
300-nm
125-nm
90-nm
60-nm
30-nm
18-nm
THR(normalized)
H(kOe)
K/K0
H_AS(kOe)
t(nm)
(b)
H(kOe)
t(nm)
H_m
ρ_TH(μΩ·cm)
-8.0E-02
-6.0E-03

Fig.4